

Extravascular Optical Coherence Tomography: Evaluation of Carotid Atherosclerosis and Pravastatin Therapy

Robert T. Wicks, Yong Huang, Kang Zhang, Mingtao Zhao, Betty M. Tyler, Ian Suk, Lee Hwang, Jacob Ruzevick, George Jallo, Henry Brem, Gustavo Pradilla and Jin U. Kang

Stroke. 2014;45:1123-1130; originally published online March 13, 2014;
doi: 10.1161/STROKEAHA.113.002970

Stroke is published by the American Heart Association, 7272 Greenville Avenue, Dallas, TX 75231
Copyright © 2014 American Heart Association, Inc. All rights reserved.
Print ISSN: 0039-2499. Online ISSN: 1524-4628

The online version of this article, along with updated information and services, is located on the World Wide Web at:

<http://stroke.ahajournals.org/content/45/4/1123>

Data Supplement (unedited) at:

<http://stroke.ahajournals.org/content/suppl/2014/03/13/STROKEAHA.113.002970.DC2.html>

Permissions: Requests for permissions to reproduce figures, tables, or portions of articles originally published in *Stroke* can be obtained via RightsLink, a service of the Copyright Clearance Center, not the Editorial Office. Once the online version of the published article for which permission is being requested is located, click Request Permissions in the middle column of the Web page under Services. Further information about this process is available in the [Permissions and Rights Question and Answer](#) document.

Reprints: Information about reprints can be found online at:
<http://www.lww.com/reprints>

Subscriptions: Information about subscribing to *Stroke* is online at:
<http://stroke.ahajournals.org//subscriptions/>

Extravascular Optical Coherence Tomography Evaluation of Carotid Atherosclerosis and Pravastatin Therapy

Robert T. Wicks, MD*; Yong Huang, PhD*; Kang Zhang, PhD; Mingtao Zhao, PhD;
Betty M. Tyler, BA; Ian Suk, CMI; Lee Hwang, MD; Jacob Ruzevick, BS; George Jallo, MD;
Henry Brem, MD; Gustavo Pradilla, MD; Jin U. Kang, PhD

Background and Purpose—Extravascular optical coherence tomography (OCT), as a noninvasive imaging methodology with micrometer resolution, was evaluated in a murine model of carotid atherosclerosis by way of assessing the efficacy of pravastatin therapy.

Methods—An OCT device was engineered for extravascular plaque imaging. Wild-type mice and apolipoprotein E-deficient ($\text{ApoE}^{-/-}$) mice were randomized to 3 treatment groups: (1) wild-type on a diet of standard rodent chow ($n=13$); (2) $\text{ApoE}^{-/-}$ on a high-fat, atherosclerotic diet (HFD; $n=13$); and (3) $\text{ApoE}^{-/-}$ on a HFD given daily pravastatin ($n=13$). Mice were anesthetized and the left common carotid was surgically exposed. Three-dimensional (3D; 2 spatial dimensions+time) and 4D (3 spatial dimensions+time) OCT images of the vessel lumen patency were evaluated. After perfusion, in situ OCT imaging was performed for statistical comparison with the *in vivo* results and final histology.

Results—Intraoperative OCT imaging positively identified carotid plaque in 100% of $\text{ApoE}^{-/-}$ mice on HFD. $\text{ApoE}^{-/-}$ mice on HFD had a significantly decreased lumen patency when compared with that in wild-type mice ($P<0.001$). Pravastatin therapy was found to increase lumen patency significantly in $\text{ApoE}^{-/-}$ mice on HFD ($P<0.01$; compared with $\text{ApoE}^{-/-}$ on HFD). The findings were confirmed with OCT imaging after perfusion and histology.

Conclusions—OCT imaging offers the potential for real-time, detailed vessel lumen evaluation, potentially improving surgical accuracy and outcomes during cerebrovascular neurosurgical procedures. Pravastatin significantly increases vessel lumen patency in the $\text{ApoE}^{-/-}$ mouse on HFD. (*Stroke*. 2014;45:1123-1130.)

Key Words: atherosclerosis ■ imaging, medical ■ intracranial aneurysm ■ tomography, optical coherence

Although subarachnoid hemorrhage from ruptured aneurysms accounts for only 5% of all strokes, it results in death in 30 to 50% of patients and plagues a population on average 20 years younger than ischemic stroke. The resulting loss of productive life years is, therefore, proportional to cerebral infarction.¹ Intracranial aneurysm formation is intimately related to extracranial carotid disease, sharing multiple risk factors and in some cases a direct causal relationship as a result of progressive atherosclerosis that inflicts increased hemodynamic stress in the nonoccluded vessels, resulting in aneurysm formation and rupture.² Although endovascular management of ruptured aneurysms is often possible, surgical clipping is frequently necessary.³ Surgical treatment of intracranial aneurysms can be challenging when severe atherosclerotic disease has affected the vicinity of the aneurysm, the aneurysmal neck, the parent vessel or the branches distal

to the aneurysm. Temporary occlusion of the parent vessel and other tributaries is required for safe surgical dissection of the aneurysm but in vessels with severe atherosclerosis, clip application may incompletely reduce flow. Similarly, complete occlusion of the aneurysm neck can be difficult if the plaque formation prevents complete occlusion during clip application. Preclipping evaluation of the vasculature involved has the potential to elucidate these problems before clip application given the surgeon valuable information to modify surgical technique and to prevent intraoperative complications.

Surgical cerebral revascularization plays an important role in certain situations of complex skull base tumors, large cerebral aneurysms, or moyamoya disease.⁴ Bypass techniques rely on the technical execution of the anastomosis performed to guarantee sufficient flow. Intraoperative evaluation of bypass patency can be performed with fluorescent video-angiography,

Received September 4, 2013; final revision received January 24, 2014; accepted January 29, 2014.

From the Departments of Neurosurgery (R.T.W., B.M.T., I.S., L.H., J.R., G.J., H.B., G.P.) and Oncology, Ophthalmology, and Biomedical Engineering (H.B.), Johns Hopkins University School of Medicine, Baltimore, MD; and Department of Electrical and Computer Engineering, Johns Hopkins University, Baltimore, MD (Y.H., K.Z., M.Z., J.U.K.).

*Drs Wicks and Huang contributed equally to the design and execution of this study and composition of the manuscript.

Presented at SPIE Photonics West, February 2013, San Francisco, CA. An early, proof-of-concept experiment was presented as an abstract at the American Association of Neurological Surgeons 2012 Conference, Miami, FL.

The online-only Data Supplement is available with this article at <http://stroke.ahajournals.org/lookup/suppl/doi:10.1161/STROKEAHA.113.002970/-DC1>.

Correspondence to Betty Tyler, BA, Department of Neurosurgery, Johns Hopkins University School of Medicine, 1550 Orleans St/CRB2-2M45, Baltimore, MD 21231. E-mail btyler@jhmi.edu

© 2014 American Heart Association, Inc.

Stroke is available at <http://stroke.ahajournals.org>

DOI: 10.1161/STROKEAHA.113.002970

conventional angiography, and Doppler measurements,⁵ but technical errors resulting in stenosis could be identified and corrected by analyzing the specific location of the stenotic segment.

Current intraoperative vascular imaging is limited to duplex ultrasonography, continuous wave Doppler, fluorescent video-angiography, or intraoperative digital subtraction angiography. Duplex ultrasonography is limited by low-definition imaging that often requires a trained ultrasonography technologist to interpret the intraoperative imaging. Continuous wave Doppler is easy to use and provides an overview of the patency of the reconstructed vessel through audible evaluation, but it is not able to provide imaging or quantify the degree of vessel stenosis.⁶ Fluorescent video-angiography, although often providing real-time visualization of small perforating vessels, image quality can be poor in deep surgical fields.⁷ Intraoperative angiography is the gold standard for imaging but has the disadvantage of requiring the use of arterial puncture and bringing in a separate angiography team into the operating room.⁸

A real-time, detailed imaging methodology of the cerebral vasculature in neurosurgical procedures can significantly affect patient outcomes.

Optical coherence tomography (OCT) could play an important role as an adjuvant intraoperative technique. OCT uses reflected infrared light, similar to the reflected sound waves found in ultrasound, to acquire real-time, cross-sectional images.⁹ The benefit of OCT is that it provides resolutions of 5 to 10 μm when compared with the resolution of several hundred micrometers found with ultrasound. Endovascular OCT imaging can resolve the normal human arterial wall structure, including the borders between adventitia, media, and intima.¹⁰ Imaging of vascular plaques has been shown to resolve the thin fibrous caps thought to be responsible for plaque vulnerability in addition to the ability to differentiate between lipid, calcium, and fibrous tissue.¹¹ Endovascular OCT, however, involves imaging with a percutaneous arterial catheter. To obtain adequate vascular wall visualization *in vivo*, blood must be displaced with saline. Optimal imaging, therefore, is limited to 2 seconds without balloon occlusion of the vessel being imaged. This requirement limits the practical application of endovascular OCT during open carotid endarterectomy or cerebrovascular surgery.

The apolipoprotein E-deficient (ApoE^{-/-}) murine model has been established as one of the closest representations of clinical atherosclerosis in humans, modeling such aspects as plaque rupture in a similar pattern as the human pathology.¹² ApoE^{-/-} mice that fed a high-fat diet (HFD) have been shown to develop arterial plaques consistently throughout the arterial system.¹³ Pravastatin therapy in combination with the model has been shown to reduce brachiocephalic artery plaque cross-sectional area by 61% and the incidence of acute plaque rupture by 36%.¹² The mouse carotid also provides a close clinical correlate to human cerebral microvasculature in both vessel wall thickness and similar hemoglobin and hematocrit % to humans.¹⁴

We set out to develop an extravascular OCT imaging device for noninvasive, real-time, detailed atherosclerotic plaque and patency visualization during intracranial vascular surgery. After development of the OCT imaging device, its accuracy in analyzing the presence of arterial plaques was assessed in the ApoE^{-/-} model. Mice were randomized to wild-type mice on a

regular diet, ApoE^{-/-} mice on a HFD to promote plaque development, and ApoE^{-/-} mice on a HFD with pravastatin therapy to inhibit plaque development and acute plaque rupture. To our knowledge, this study represents the first application of extravascular OCT imaging to assess plaque morphology and statin efficacy in a live, *in vivo* model of atherosclerosis.

Materials and Methods

Experimental Design

We set out to assess the ability of intraoperative OCT imaging to determine the presence, size, and morphology of carotid arterial plaques in a murine model of atherosclerosis accurately. A total of 39 wild-type and ApoE^{-/-} mice in 2 separate experiments were placed into 1 of the 3 groups to compare plaque development and morphology. Wild-type mice (n=13) were provided a standard rodent diet. ApoE^{-/-} (n=26) were provided a HFD and then randomized to 1 of the 2 treatment groups: (1) ApoE^{-/-} on HFD and (2) ApoE^{-/-} on HFD with daily pravastatin.

Study 1 consisted of a proof of concept analysis to establish the OCT imaging methodology, to analyze plaque development over time to establish the optimal timing of carotid plaque development, and to determine the survivability of the surgical procedure. In the first experiment, OCT imaging was obtained at 8 weeks (n=1 per group), 10 weeks (n=1 per group), and 14 weeks (n=3 per group). After left lateral neck dissection and OCT imaging were completed, the mice were either kept alive for a second imaging or were euthanized and perfused. After perfusion, the carotid arteries were again imaged *in situ* for comparison of plaque morphology with the live, *in vivo* images. A final feasibility experiment in study 1 was then performed by converting the table-top, stationary OCT unit (Figure 1) into a handheld imaging probe adapted for clinical application (Figure 1, inset; Figure I in the online-only Data Supplement); the details of which have been previously published.¹⁵ The probe used a stainless steel handpiece and had a 2-cm working distance. Mice at 10 weeks were imaged using the handheld probe before perfusion.

Study 2 was performed using the benchtop OCT device to establish the efficacy of OCT imaging to determine plaque presence and size when compared with histology and to determine the treatment efficacy of pravastatin therapy. Mice (n=8 per group) were administered their designated treatments for 14 weeks followed by live, *in vivo* OCT imaging and postperfusion *in situ* OCT imaging. The carotid arteries were then resected, and the histology obtained was compared with the OCT images. Acquired cross-sectional OCT images and histology slices were evaluated for percent lumen patency by highlighting the region of patent inner vessel lumen excluding plaque and calculating the highlighted area using ImageJ software (Rasband W.S.; ImageJ; U. S. National Institutes of Health, Bethesda, MD; <http://imagej.nih.gov/ij/>, 1997–2012). The percent lumen patency was reported as mean±SEM.

Animals

C57BL/6J wild-type mice (Jackson Laboratories, Bar Harbor, ME) and C57BL/6J ApoE^{-/-} mice (Jackson Laboratories) of 10 weeks were taken for the initial experiment and 18 weeks for the final experiment. All mice were housed in standard animal facilities with free access to Baltimore City water. Wild-type mice were given free access to standard rodent chow. ApoE^{-/-} mice were given free access to HFD, atherogenic rodent diet (Harlan Laboratories, Indianapolis, IN). The Johns Hopkins Animal Care and Use Committee approved all experimental protocols.

Design of the OCT Imaging Device

Details of the OCT system configuration were reported in our previous work.^{16–18} The system used a light source of wavelength 825 nm, as we found this to provide the optimal balance of image resolution and light scattering for imaging murine carotid atherosclerosis based on previous experiments trialing both 825 and 1300 nm

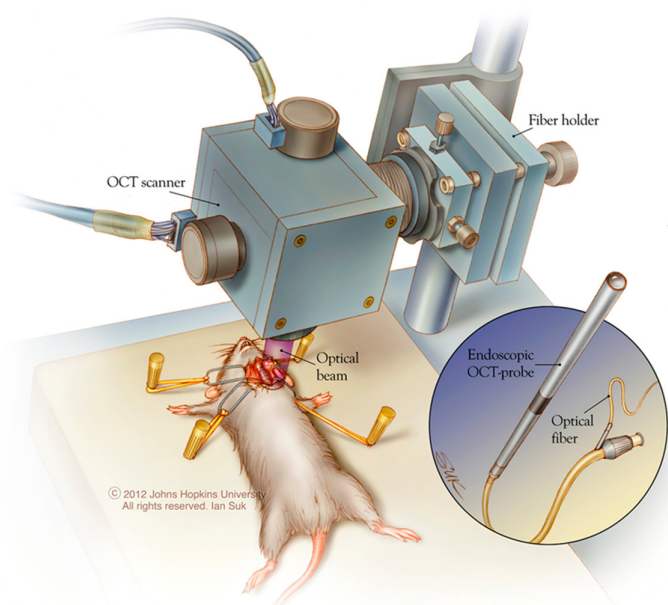
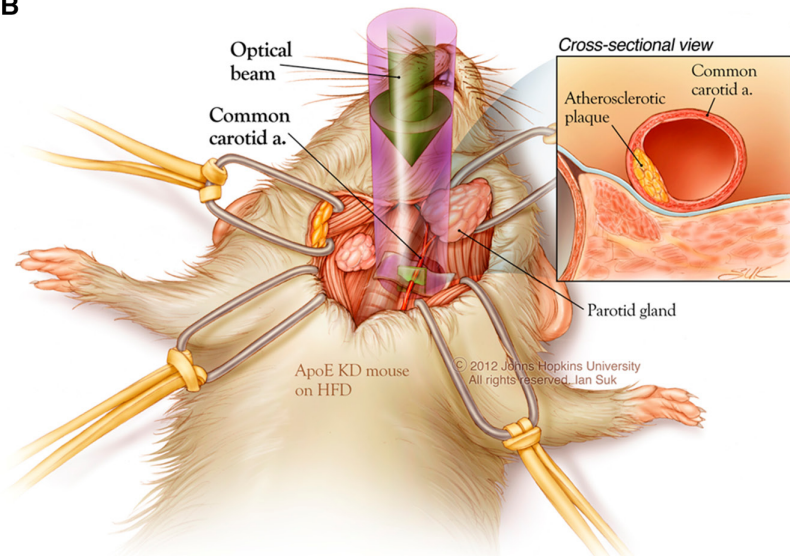
A**B**

Figure 1. **A**, Schematic of experimental setup. The complementary metal-oxide-semiconductor camera of the spectrometer was set to operate at 1024-pixel mode by selecting the area of interest. The minimum line period was camera limited to 7.8 μ s with the exposure time of 6.5 μ s, corresponding to a maximum line rate of 128000 A-scan/s. The scanning rate is 2.3 (X) by 2.3 mm (Y) lateral and 3 mm (Z) for the axial full-range. Each B-mode image consisted of 512 A-lines. The figure inset diagrams the proof of concept optical coherence tomography (OCT) imaging probe for use during cerebrovascular neurosurgical procedures and endoscopic skull base surgery. **B**, Details of OCT cross-sectional imaging of the apolipoprotein E-deficient (ApoE knockdown [KD]) mouse on high-fat diet (HFD) left common carotid artery bifurcation. The obtained cross-sectional images were used to reconstruct 4-dimensional (3 spatial dimensions with time; Figure 5) diagrams simultaneously using the dual-graphics processing unit computing architecture.

(Figure II in the online-only Data Supplement). The OCT system is built on a dual-graphics processing unit computer architecture, which allows for cross-sectional imaging with simultaneous ultrafast 4-dimensional (4D; 3 spatial dimensions with time) reconstruction. The OCT spectrometer was set to operate at 1024-pixel mode by selecting the area of interest. The minimum line period was spectrometer limited to 7.8 μ s with the exposure time of 6.5 μ s, corresponding to a maximum line rate of 128000 A-scan/s. The imaging volume is 2.3 (X) by 2.3 mm (Y) lateral and 3 mm (Z) axial. Each B-mode image consisted of 512 A-lines. The system has a measured axial resolution of 6 μ m in air and lateral resolution was \approx 20 μ m assuming Gaussian beam profile.

Anesthesia

Mice were anesthetized with a single intraperitoneal injection (0.05 mL/10 g) of an anesthetic mixture containing xylazine (10 mg/kg; 100 mg/mL Xyla-ject; Phoenix Pharmaceutical, Inc, St. Joseph, MO) and ketamine (50 mg/kg; 100 mg/mL KetaThesia; Butler Animal Health Supply, Dublin, OH). The absence of pedal and tail pinch reflexes was confirmed before the procedure performance.

Surgical Technique

After initiation of anesthesia, the midline and left neck were shaved (Chromini Cordless Trimmer; Wahl Manufacturing Co, Toronto, Canada). The region was then scrubbed with povidone-iodine topical antiseptic followed by 70% ethyl alcohol. Mice were placed supine, and a vertical skin incision was made in the skin overlying the left neck approximating the location of the left carotid sheath. The underlying soft tissue and salivary glands were dissected with the use of a surgical microscope (Carl Zeiss Co, Oberkochen, Germany). Four miniaturized retractors were placed to retract the submaxillary gland, sternocleidomastoid muscle, and midline strap muscles to reveal the region of the carotid sheath. The left common carotid artery was bluntly separated from the surrounding tissue and was visualized to above the level of the carotid bifurcation. A small piece of latex measuring 3 \times 5 mm was then placed under the distal common carotid and proximal bifurcation to maintain visualization during the imaging process in a similar manner to those used during cerebrovascular bypass procedures.

After *in vivo* OCT imaging of the live mice was completed, the mice were separated into those who were to remain alive for a follow-up imaging procedure (n=3 per group), performed only during

study 1, and the remaining underwent perfusion to undergo postperfusion imaging. Mice designated to remain alive for additional imaging had the latex piece removed, tissues reapproximated, and the incision closed using a 4-0 silk suture (Ethicon, Sommerville, NJ).

OCT Imaging Acquisition and Analysis

After left carotid exposure, the extravascular OCT scanner was placed over the distal common carotid to capture plaque development at the carotid bifurcation (Movie IA and IIA in the online-only Data Supplement). There were 2 imaging modes of the OCT system: B-mode and C-mode imaging. The OCT system ran at 128000 A-scans/s. Under B-mode imaging mode, cross-sectional image of a specific area of interest under investigation by the surgeon was obtained. Each raw B-mode image consisted of 512 A-scans covering a reasonable whole vessel diameter. Every 10 frames were averaged to improve the image quality, which gives an effective imaging video rate of 25 frames per second (fps), from an initial rate of 250 fps. Another advantage of averaging the frames is that speckle patterns, which are inherent with OCT images, are averaged out for blood flow, whereas plaque and vessel wall images contained a pronounced grain pattern.¹⁹ This information was used to determine which part was plaque and which part was blood within the vessel wall. For C-mode imaging, each volume consisted of 500 B-frames. Although real-time images were rendered, raw spectra data for the B-mode and C-mode images were also saved for later analysis, if needed. Image processing software, ImageJ, was used to perform the postimage processing and volume rendering.

Tissue Preparation

After completion of OCT imaging, mice were perfused via bilateral thoracotomy, cannulation of the left ventricle, and opening of the right atrium. Perfusion was performed with 50 mL of normal saline (0.9% NaCl) at 10 mL/min using a pump (Watson-Marlow, Inc, Wilmington, MA). The saline was followed by perfusion with 50 mL of 10% formalin at 10 mL/min. Injection of porcine gelatin (Sigma Aldrich, St. Louis, MO) was then performed via syringe injection through the previously placed cannula within the left ventricle. The mice then underwent *in situ*, extravascular OCT imaging for comparison with the previous live, *in vivo* imaging (Movies IB and IIB in the online-only Data Supplement).

After completion of the *in situ* imaging, the carotid artery was excised from the level 10 mm proximal to the common carotid bifurcation to the level 1 mm distal to the bifurcation. A 4-0 silk suture tie was placed at the proximal end for identification during histological slicing. The excised carotid arteries were labeled and placed in 10% formalin for >48 hours for fixation and embedded in paraffin. Five axial sections of 10- μ m thickness were taken at the carotid bifurcation at 5 levels separated by 100 μ m. Samples were then processed and placed on glass slides. One slide from each level was then stained with hematoxylin and eosin. The level found to be nearest the midpoint of the carotid bifurcation was then independently identified and used for comparison analysis with OCT imaging.

Inter-Rater Reliability

To determine the potential clinical application of intraoperative OCT imaging of atherosclerotic plaques better, a brief test was designed to assess the ease of identifying plaque on single-frame, cross-sectional images obtained from live mice. A 1-page instruction sheet consisting of 4 cross-sectional images, 2 containing no plaque and 2 containing carotid plaque with the plaque identified by outline and arrows, was initially provided to the volunteers. After this brief instruction page, 4 blinded volunteers were asked to identify whether plaque was present in a series of 24 printed OCT images obtained *in vivo* from live study mice. The volunteers had varying levels of experience with interpreting OCT images from no exposure to experienced.

Statistical Analysis

Analysis of percent lumen patency between treatment groups using a single imaging modality (*live*, *in vivo* OCT imaging; postperfusion

OCT imaging, histological imaging) was performed using a Kruskal-Wallis test (1-way, nonparametric ANOVA). Statistical significance of the difference in percent lumen patency between imaging modalities was calculated using the Friedman test (nonparametric, repeated measures ANOVA). Inter-rater reliability was calculated as mean \pm SEM sensitivity and specificity. All calculations were performed using GraphPad Prism version 6.00 for Macintosh (GraphPad Software, La Jolla, CA).

Results

OCT Image Acquirement

OCT imaging was acquired in a total of 38 wild-type and ApoE^{-/-} mice. Study 1 consisted of a total of 15 mice within the 3 treatment groups imaged over time for proof of concept

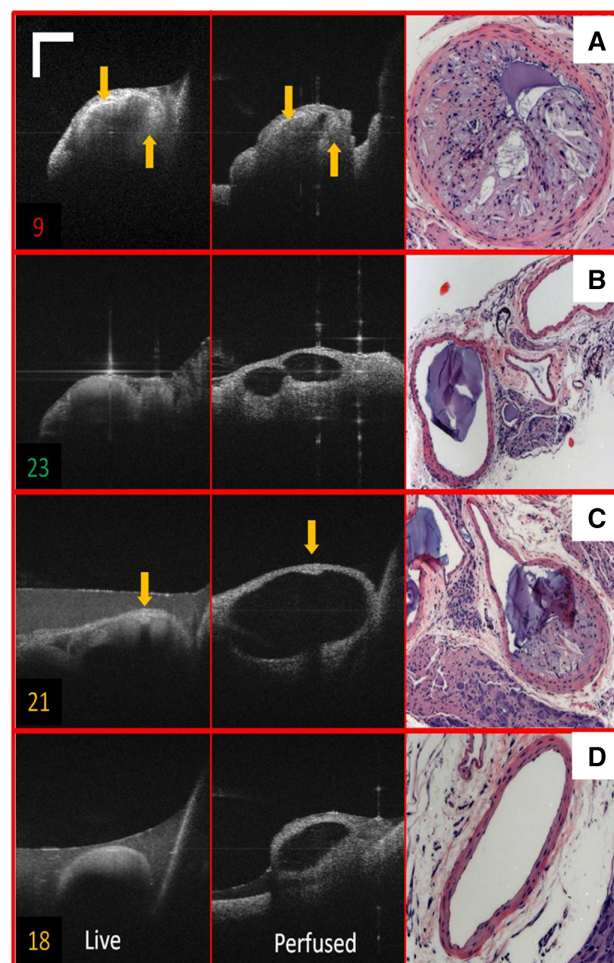


Figure 2. Typical cross-sectional optical coherence tomography (OCT) images of the carotid artery within the 3 treatment groups compared with histology. Mouse number is labeled in color at the bottom left of each row: green (A) indicates wild-type mice on regular diet, red (B) indicates apolipoprotein E-deficient (ApoE^{-/-}) mice on high-fat diet (HFD), and yellow (C, D) indicates ApoE^{-/-} mice on HFD with pravastatin treatment. The first image of each figure is obtained during live, *in vivo* imaging. The second image is captured *in situ* after perfusion. The third image consists of hematoxylin and eosin (H&E) histological slides, stained after perfusion (scale bar, 500 μ m). The violet artifact within the lumen of the H&E slides is a result of porcine gelatin injection after artery perfusion to maintain the 3-dimensional architecture for comparison of vessel lumen patency with the obtained OCT images. Yellow arrows have been provided to assist the reader in identifying atherosclerotic plaque presence.

and determination of study methodology—group 1: wild-type mice provided a standard rodent diet ($n=5$); group 2: ApoE^{-/-} mice provided a HFD ($n=5$), and group 3: ApoE^{-/-} mice on HFD with daily pravastatin ($n=5$). Mice from each group were imaged at 8, 10, and 14 weeks to establish the time-course of plaque development in the ApoE^{-/-} mouse carotid. Plaque was initially evident at 8 weeks within the ApoE^{-/-} on HFD mice. Optimal plaque development across all imaged ApoE^{-/-} on HFD mice was seen at 14 weeks. ApoE^{-/-} mice on HFD given daily pravastatin at the time of initiation of the HFD had a lesser degree of plaque development. The OCT scanning fiber was then integrated into a handheld probe as a proof of concept of the convertibility of the imaging system into a clinically feasible handheld device for intraoperative imaging.

Study 2 was then performed to establish the statistical efficacy of extravascular OCT detection of carotid atherosclerosis when compared with histology and to establish the therapeutic efficacy of pravastatin treatment. After administration of the designated treatment for 14 weeks, mice were anesthetized and surgical exposure performed for in vivo OCT imaging, postperfusion in situ OCT imaging. The carotid arteries were then resected, and the previously obtained OCT images were compared with the histology.

Atherosclerotic Plaque Evaluation

At 14 weeks after treatment initiation, the 23 (1 ApoE^{-/-} mouse on HFD did not survive to 14 weeks) mice of study 2 underwent live, in vivo OCT imaging, postperfusion in situ OCT imaging, and ex vivo histological analysis (Figures 2 and 3).

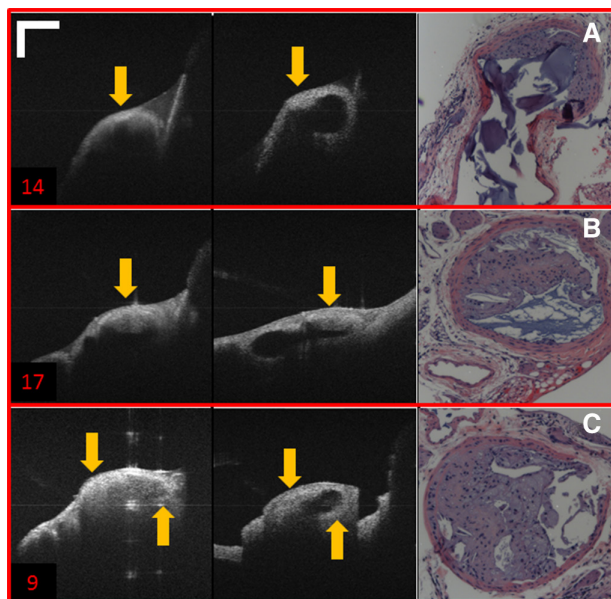


Figure 3. Carotid artery vessel lumen patency at various levels within the apolipoprotein E-deficient mouse on high-fat diet, mouse label number was marked on the bottom left: (A) level 1: 100% to 80% lumen patency; (B) level 2: 80% to 50% lumen patency; (C) level 3: 50% to 0% lumen patency (scale bar, 500 μ m). The violet artifact within the lumen of the H&E slides is a result of porcine gelatin injection after artery perfusion to maintain the 3-dimensional architecture for comparison of vessel lumen patency with the obtained optical coherence tomography (OCT) images.

When placed in direct comparison with the perfused arteries, the scattering component of RBCs results in suboptimal imaging of the far wall of the carotid artery. Despite this limitation, the presence of carotid plaque was identified during OCT imaging in 100% of ApoE^{-/-} on HFD mice before perfusion. When compared with histology, OCT real-time video captured before perfusion, when evaluated by 2 researchers experienced in OCT, revealed 100% sensitivity and 100% specificity for plaque identification in both the ApoE^{-/-} on HFD group and the ApoE^{-/-} on HFD with pravastatin group.

The mean percentage lumen patency (Figure 4) in ApoE^{-/-} on HFD mice was found to be 74.9% (± 6.8), significantly less than that of normal mice ($P<0.001$) in which all were found to have 100% lumen patency and ApoE^{-/-} on HFD with pravastatin ($P<0.01$), which were identified to have 97.1% (± 5.8) lumen patency. In comparison with postresection histology, mean percentage luminal patency in ApoE^{-/-} on HFD mice was found to be significantly less during live, in vivo imaging than those on postresection histology ($P<0.01$). ApoE^{-/-} mice on HFD revealed a 74.9% (± 6.8) lumen patency in live mice in comparison with a 41.4% (± 8.6) lumen patency noted on histology. With normal mice and ApoE^{-/-} on HFD with pravastatin, no significant difference was noted between live, in vivo OCT imaging and postperfusion histology.

Inter-Rater Reliability of Plaque Presence

After completion of the standardized volunteer assessment of single cross-sectional images, the mean sensitivity of live, in vivo OCT imaging in identifying plaque presence was 86.25% (± 8.25) and specificity was 71.50% (± 9.17).

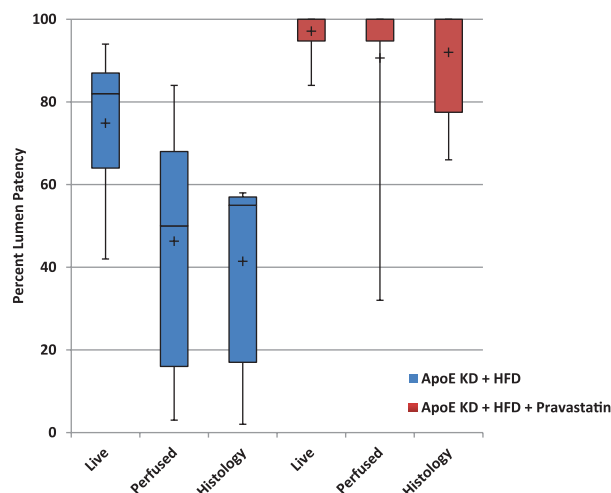


Figure 4. Percentage lumen patency of the murine carotid artery, as calculated by live, intraoperative optical coherence tomography (OCT) imaging (live); postperfusion OCT imaging (perfused); and histology. The area of patent vessel lumen is presented for each mouse within the apolipoprotein E knockdown (ApoE KD) on high-fat diet (HFD) group and the ApoE KD on HFD with pravastatin treatment group. Box plot symbols are as follows: +, mean; -, median; □, 75th percentile, 25th percentile; ↑, 100th percentile; and ↓, 0th percentile. Within the ApoE KD+HFD group, mean percentage lumen patency was found to be significantly less by postperfusion OCT imaging and histology than by the intraoperative OCT imaging. The ApoE KD+HFD+pravastatin group was found to have significantly greater mean percentage lumen patency than the ApoE KD+HFD using all 3 measurement modalities.

En Face and 4D Reconstruction

To assess the clinical potential of intraoperative OCT imaging further, our OCT system was engineered to provide simultaneous volume rendering of the scanned images to present the plaque morphology and optimize the ability to determine the extent of atherosclerotic plaque within a vessel. From a 4D volume C-scan image, en face slices at varying depths were obtained to visualize plaque during the live, in vivo imaging and the postperfusion *in situ* imaging (Figure 5). Figure 6A reveals live, in vivo vessel imaging with partial atherosclerotic plaque occlusion. Figure 6B depicts a normal vessel wall after perfusion and reveals a virtually simultaneous reconstruction of the common carotid bifurcation into the internal and external carotid arteries. Figure 6C shows a heavily occluded vessel after perfusion. To study the inner plaque volumetric morphology better, 2 virtual cut views can be made by cutting the vessel into top and bottom halves.

Discussion

This study describes the use of extravascular OCT imaging in the intraoperative evaluation of carotid plaque in ApoE^{-/-} mice and reports the first use of extravascular OCT to analyze pravastatin efficacy in preventing plaque development in live mice. The presence of atherosclerotic carotid plaque was positively identified by OCT imaging in 100% of ApoE^{-/-} mice on HFD, when analyzing real-time video. On analysis of plaque morphology, live, in vivo OCT imaging in ApoE^{-/-} mice on HFD had a statistically significant decrease in vessel lumen patency when compared with that in wild-type mice. Pravastatin therapy was found to increase the carotid artery

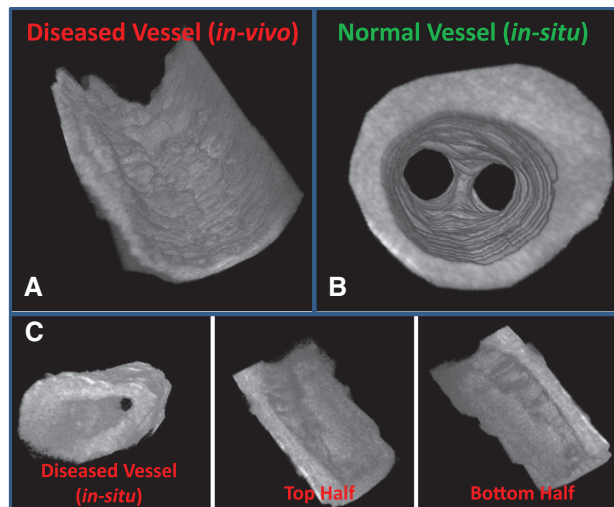


Figure 6. Four-dimensional volume rendering of the vessels. **A**, An in vivo partially occluded vessel; **(B)** a normal hollow vessel after perfusion; **(C)** a heavily occluded vessel after perfusion with the top and bottom half of vessel revealed through virtual cut.

lumen patency significantly in ApoE^{-/-} mice on HFD. This statistically significant increase in vessel lumen patency was evident on live, in vivo OCT imaging and confirmed by postperfusion *in vitro* OCT imaging and histology.

A standardized assessment containing 24 randomized OCT images of live, in vivo carotids from all 3 treatment groups was then presented to a group of volunteers with a diversity of experience with OCT images from zero to experienced. Although presented with a single cross-sectional carotid image rather than a dynamic, live video with 4D reconstruction, which would be available during live imaging, the assessment revealed a mean sensitivity of 86.3% and specificity of 71.5%. Given the presence of the added limitation of erythrocyte scattering seen with in vivo OCT imaging, this sensitivity compares favorably with that of the ex vivo, perfused analysis of human coronary plaque by intravascular OCT by Rieber et al,²⁰ which revealed a sensitivity ranging from 64% to 77% and specificity of 88% to 97%. Likewise, Manfrini et al²¹ reported a sensitivity of 45% to 83% and specificity of 76% to 83% for clinical intravascular OCT imaging. In comparison, our OCT imaging during study 2 revealed 100% sensitivity and specificity for carotid plaque detection when live, in vivo imaging was compared with postperfusion histology.

Our purpose in this study was to establish whether OCT imaging would provide an effective technique for high-definition, live imaging that would assist intraoperative decision making during cerebrovascular procedures. Recent research interest has focused on the ability of endovascular OCT imaging of atherosclerotic plaques to provide information on plaque morphology and possibly assist in predicting plaque rupture vulnerability.^{22,23} Although endovascular OCT imaging may have diagnostic potential, its intraoperative application is limited. Its requirement for invasive, intravascular catheter placement requires the equipment and expertise of a physician experienced in endovascular techniques, adding to the time and cost of a potential surgical procedure. In addition, the securing of cerebral aneurysms and performing

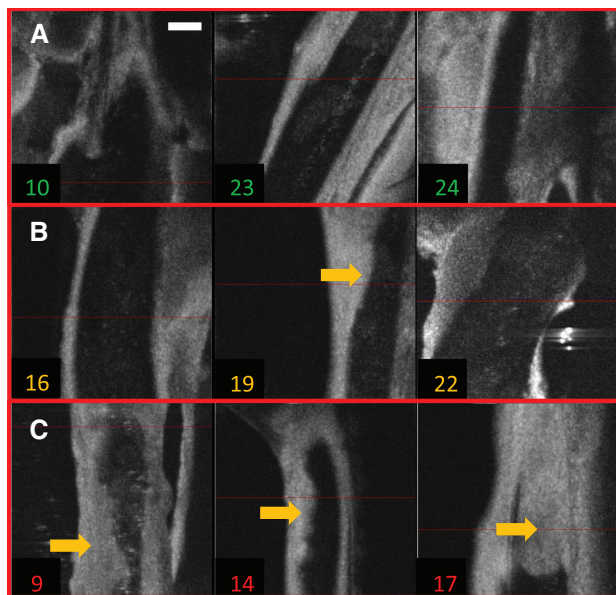


Figure 5. En face slices (screen captured with red line indicating optical coherence tomography scanning beam) at different depths to visualize the carotid plaque from different mice after perfusion, mouse label number was marked in color at the bottom left, green (**A**) indicates wild-type mice on regular diet, yellow (**B**) indicates apolipoprotein E-deficient (ApoE^{-/-}) mice on high-fat diet (HFD) with pravastatin treatment, and red (**C**) indicates ApoE^{-/-} mice on HFD without treatment (scale bar for both horizontal and vertical directions, 500 μ m).

cerebrovascular bypass procedures requires the use of intraoperative temporary arterial clipping, precluding the simultaneous use of an endovascular catheter.²⁴

The greatest benefit to date of OCT image acquisition instead of intraoperative ultrasound is the high-definition imaging possible that enables detailed 4D (3 spatial dimensions plus time) reconstruction of the vessel lumen. With the dual-graphics processing unit system engineered for our present device, we were able to produce virtual-live 4D images that could be used to make instantaneous intraoperative decisions without need for an invasive procedure, such as intravascular catheter insertion. In addition, many OCT imaging devices have been limited by a frame capture rate of 4 to 8 fps found in initial studies^{11,25} with ≤100 fps on current commercial units.²⁶ Our dual-graphics processing unit system captures 250 fps and averages every 10 frames. Speckle patterns, which are inherent with OCT images, are averaged out as blood flow, whereas plaque and vessel wall images remain stable. The averaging, therefore, removes much of the motion artifact found in a live pulsating object, such as the mouse carotid artery, enabling clearer visualization of the plaque morphology. In addition, the ability of this system to be integrated into a handheld imaging probe allows for free-range imaging of the vessel lumen from multiple angles.

The most apparent limitation of OCT imaging is the depth of light penetration, between 0.5 and 3 mm with most systems used clinically today. Depth of light penetration is directly related to the wavelength selected and becomes a trade-off between light absorption and scattering. Absorption is minimized within tissue between the wavelengths of 700 and 1300 nm. Although absorption is lower at 700 nm, scattering is less at 1300 nm, which leads to greater tissue penetration at longer wavelengths. For our system, we used a light source of wavelength 825 nm because we found that this to provide the optimal balance of tissue penetration and scattering for imaging murine carotid atherosclerosis (sample pre-experiment study comparing *in vivo* imaging of the same murine carotid artery with an 825 nm versus 1300 nm system is seen in Figure II in the online-only Data Supplement). This choice of wavelength, however, did limit our depth of penetration to ≈1 mm. The depth of penetration would limit immediate clinical application in certain surgical procedures, such as carotid endarterectomy, where the average total wall thickness without diseased plaque is 1.05 mm.²⁷ One potential method of overcoming this limitation is through the use of the prototype handheld OCT imaging probe. Holding the probe from 3 different angles at 0°, 90°, and 180°, for example, could provide for a virtual 360° image reconstruction of the vessel lumen. Also, the depth of tissue penetration is less of an issue within the field of vascular neurosurgery, such as aneurysm securing procedures, where the integration of our current system into a handheld imaging probe may have immediate clinical application. For example, arguably some of the most complex of cerebral aneurysms to secure with an open surgical approach involve the anterior communicating artery. The average total diameter of human anterior communicating artery is 1.5 mm with total wall thickness much less, which is within the 1-mm depth of penetration using our current OCT imaging system.²⁸ An OCT imaging probe would allow for evaluation of the

vessel lumen after aneurysm securing, immediately ensuring that no nearby perforating arteries are unknowingly occluded by the aneurysm clip. Intraoperative occlusion of small perforating vessels has been estimated to account for 8% of all strokes after clipping of ruptured cerebral aneurysms.²⁹

Conclusions

OCT evaluation of the carotid artery in ApoE^{-/-} mice on HFD revealed a statistically significant decrease in lumen patency when compared with that in wild-type mice on a regular diet. Pravastatin was found to significantly increase vessel lumen patency in the ApoE^{-/-} mouse on HFD. OCT offers the potential for real-time, detailed vessel lumen evaluation with simultaneous 4D reconstruction, potentially improving surgical accuracy and outcomes during cerebrovascular neurosurgical procedures.

Acknowledgments

Drs Wicks and Huang contributed equally to the design and execution of this study and composition of the article. Dr Huang acknowledges the China Scholarship Council (CSC) for its support of his PhD study. We would like to thank Ali and Peter Jennison for their generous support of this research.

Sources of Funding

This work was supported by National Institutes of Health grant R21 1R21NS063131-01A1.

Disclosures

None.

References

1. Johnston SC, Selvin S, Gress DR. The burden, trends, and demographics of mortality from subarachnoid hemorrhage. *Neurology*. 1998;50:1413–1418.
2. Hashimoto T, Meng H, Young WL. Intracranial aneurysms: links among inflammation, hemodynamics and vascular remodeling. *Neurol Res*. 2006;28:372–380.
3. Spetzler RF, McDougall CG, Albuquerque FC, Zabramski JM, Hills NK, Partovi S, et al. The Barrow Ruptured Aneurysm Trial: 3-year results. *J Neurosurg*. 2013;119:146–157.
4. Berg-Johnsen J, Helseth E, Langmoen IA. Cerebral revascularization for skull base tumors. *World Neurosurg*. March 28, 2013. doi:10.1016/j.wneu.2013.03.052. [http://www.worldneurosurgery.org/article/S1878-8750\(13\)00546-9/fulltext](http://www.worldneurosurgery.org/article/S1878-8750(13)00546-9/fulltext). Accessed July 21, 2013.
5. Schuette AJ, Dannenbaum MJ, Cawley CM, Barrow DL. Indocyanine green videoangiography for confirmation of bypass graft patency. *J Korean Neurosurg Soc*. 2011;50:23–29.
6. Rockman CB, Halm EA. Intraoperative imaging: does it really improve perioperative outcomes of carotid endarterectomy? *Semin Vasc Surg*. 2007;20:236–243.
7. Gruber A, Dorfer C, Standhardt H, Bavinzski G, Knosp E. Prospective comparison of intraoperative vascular monitoring technologies during cerebral aneurysm surgery. *Neurosurgery*. 2011;68:657–73, discussion 673.
8. Lee CH, Jung YS, Yang HJ, Son YJ, Lee SH. An innovative method for detecting surgical errors using indocyanine green angiography during carotid endarterectomy: a preliminary investigation. *Acta neurochirurgica*. 2012;154:67–73, discussion 73.
9. Huang D, Swanson EA, Lin CP, Schuman JS, Stinson WG, Chang W, et al. Optical coherence tomography. *Science*. 1991;254:1178–1181.
10. Kohno H, Sueda S, Sakae T. Separation of the intima-media complex from the adventitia during spontaneous coronary artery spasm documented by intracoronary optical coherence tomography. *Int J Cardiol*. 2012;154:e4–e5.
11. Jang IK, Bouma BE, Kang DH, Park SJ, Park SW, Seung KB, et al. Visualization of coronary atherosclerotic plaques in patients using

- optical coherence tomography: comparison with intravascular ultrasound. *J Am Coll Cardiol.* 2002;39:604–609.
12. Johnson J, Carson K, Williams H, Karanam S, Newby A, Angelini G, et al. Plaque rupture after short periods of fat feeding in the apolipoprotein E-knockout mouse: model characterization and effects of pravastatin treatment. *Circulation.* 2005;111:1422–1430.
 13. Nakashima Y, Plump AS, Raines EW, Breslow JL, Ross R. ApoE-deficient mice develop lesions of all phases of atherosclerosis throughout the arterial tree. *Arterioscler Thromb.* 1994;14:133–140.
 14. Lockner D, Sletten K, de Hevesy G. Studies on cancer anaemia: organ weights, blood values and iron metabolism in normal and tumour-bearing mice. *Br J Cancer.* 1963;17:328–354.
 15. Zhang K, Huang Y, Kang JU. Full-range fourier domain optical coherence tomography imaging probe with a magnetic-driven resonant fiber cantilever. *Opt Eng.* 2011;50:119002.
 16. Zhang K, Kang JU. Real-time intraoperative 4D full-range FD-OCT based on the dual graphics processing units architecture for microsurgery guidance. *Biomed Opt Express.* 2011;2:764–770.
 17. Kang JU, Huang Y, Zhang K, Ibrahim Z, Cha J, Lee WP, et al. Real-time three-dimensional Fourier-domain optical coherence tomography video image guided microsurgeries. *J Biomed Opt.* 2012;17:081403–081401.
 18. Huang Y, Liu X, Kang JU. Real-time 3D and 4D Fourier domain Doppler optical coherence tomography based on dual graphics processing units. *Biomed Opt Express.* 2012;3:2162–2174.
 19. Mariampillai A, Standish BA, Moriyama EH, Khurana M, Munce NR, Leung MK, et al. Speckle variance detection of microvasculature using swept-source optical coherence tomography. *Opt Lett.* 2008;33:1530–1532.
 20. Rieber J, Meissner O, Babaryka G, Reim S, Oswald M, Koenig A, et al. Diagnostic accuracy of optical coherence tomography and intravascular ultrasound for the detection and characterization of atherosclerotic plaque composition in ex-vivo coronary specimens: a comparison with histology. *Coron Artery Dis.* 2006;17:425–430.
 21. Manfrini O, Mont E, Leone O, Arbustini E, Eusebi V, Virmani R, et al. Sources of error and interpretation of plaque morphology by optical coherence tomography. *Am J Cardiol.* 2006;98:156–159.
 22. Tahara S, Morooka T, Wang Z, Bezerra HG, Rollins AM, Simon DI, et al. Intravascular optical coherence tomography detection of atherosclerosis and inflammation in murine aorta. *Arterioscler Thromb Vasc Biol.* 2012;32:1150–1157.
 23. Jang IK, Tearney GJ, MacNeill B, Takano M, Moselewski F, Iftima N, et al. In vivo characterization of coronary atherosclerotic plaque by use of optical coherence tomography. *Circulation.* 2005;111:1551–1555.
 24. Samson D, Batjer HH, Bowman G, Mootz L, Krippner WJ Jr, Meyer YJ, et al. A clinical study of the parameters and effects of temporary arterial occlusion in the management of intracranial aneurysms. *Neurosurgery.* 1994;34:22–8, discussion 28.
 25. Yabushita H, Bouma BE, Houser SL, Aretz HT, Jang IK, Schlendorf KH, et al. Characterization of human atherosclerosis by optical coherence tomography. *Circulation.* 2002;106:1640–1645.
 26. Ughi GJ, Adriaenssens T, Desmet W, D'hooge J. Fully automatic three-dimensional visualization of intravascular optical coherence tomography images: methods and feasibility in vivo. *Biomed Opt Express.* 2012;3:3291–3303.
 27. Gamble G, Beaumont B, Smith H, Zorn J, Sanders G, Merrilees M, et al. B-mode ultrasound images of the carotid artery wall: correlation of ultrasound with histological measurements. *Atherosclerosis.* 1993;102:163–173.
 28. Perlmutter D, Rhon AL Jr. Microsurgical anatomy of the anterior cerebral-anterior communicating-recurrent artery complex. *J Neurosurg.* 1976;45:259–272.
 29. Hoh BL, Curry WT Jr, Carter BS, Ogilvy CS. Computed tomographic demonstrated infarcts after surgical and endovascular treatment of aneurysmal subarachnoid hemorrhage. *Acta Neurochir (Wien).* 2004;146:1177–1183.

SUPPLEMENTAL MATERIAL

Extravascular Optical Coherence Tomography: Evaluation of Carotid Atherosclerosis and Pravastatin Therapy

Authors

Robert T. Wicks, MD^{1*}, Yong Huang, PhD^{2*}, Kang Zhang, PhD², Mingtao Zhao, PhD², Betty M. Tyler, BA¹, Ian Suk, CMI¹, Lee Hwang, MD¹, Jacob Ruzevick, BS¹, George Jallo, MD¹, Henry Brem, MD^{1,3}, Gustavo Pradilla, MD¹, and Jin U. Kang, PhD²

Department of Neurosurgery¹, Johns Hopkins University School of Medicine, Baltimore, Maryland; Department of Electrical and Computer Engineering², Johns Hopkins University, Baltimore, Maryland; Departments of Oncology, Ophthalmology, and Biomedical Engineering³, Johns Hopkins University School of Medicine, Baltimore, Maryland

*Authors RTW and YH contributed equally to the design and execution of this study and composition of the manuscript.

Correspondence and Reprint Requests to:

Betty Tyler

Department of Neurosurgery

Johns Hopkins University School of Medicine

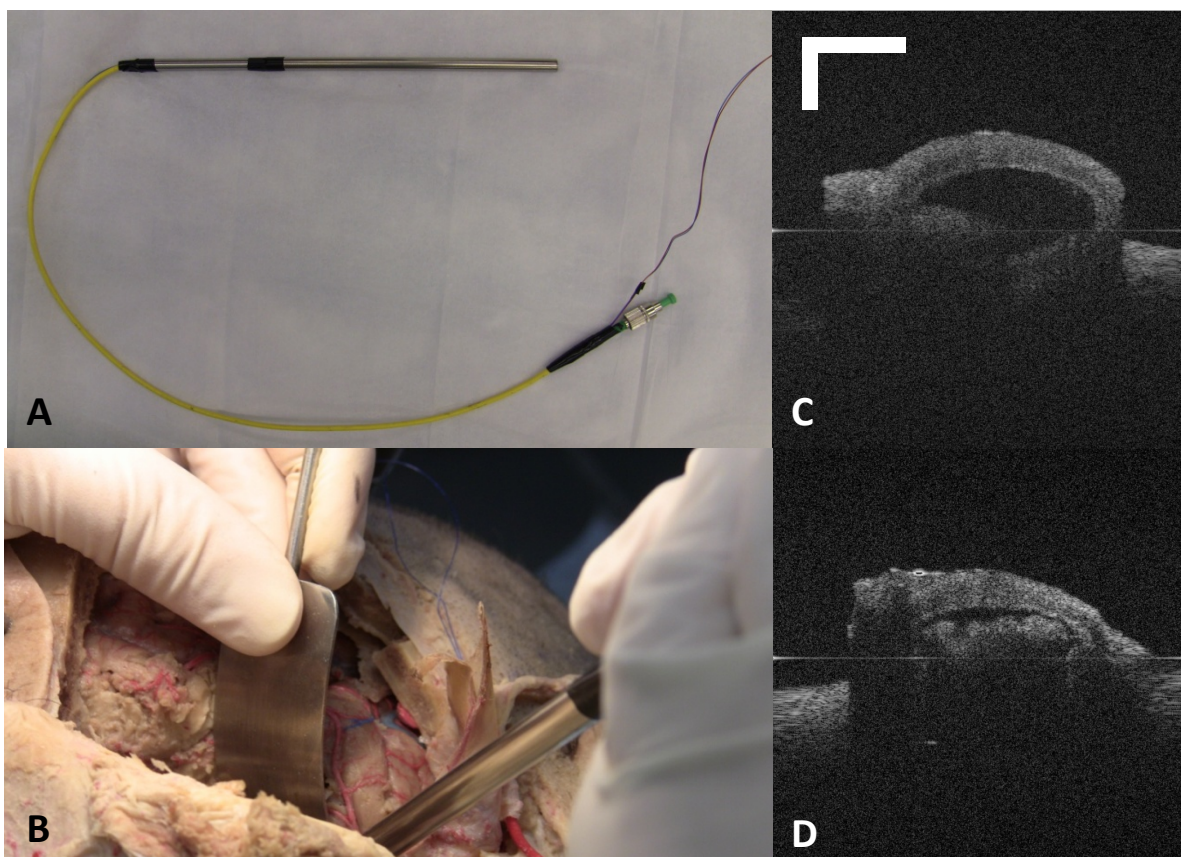
1550 Orleans Street/CRB2-2M45

Baltimore, Maryland 21231 USA

Phone- 410-502-8197

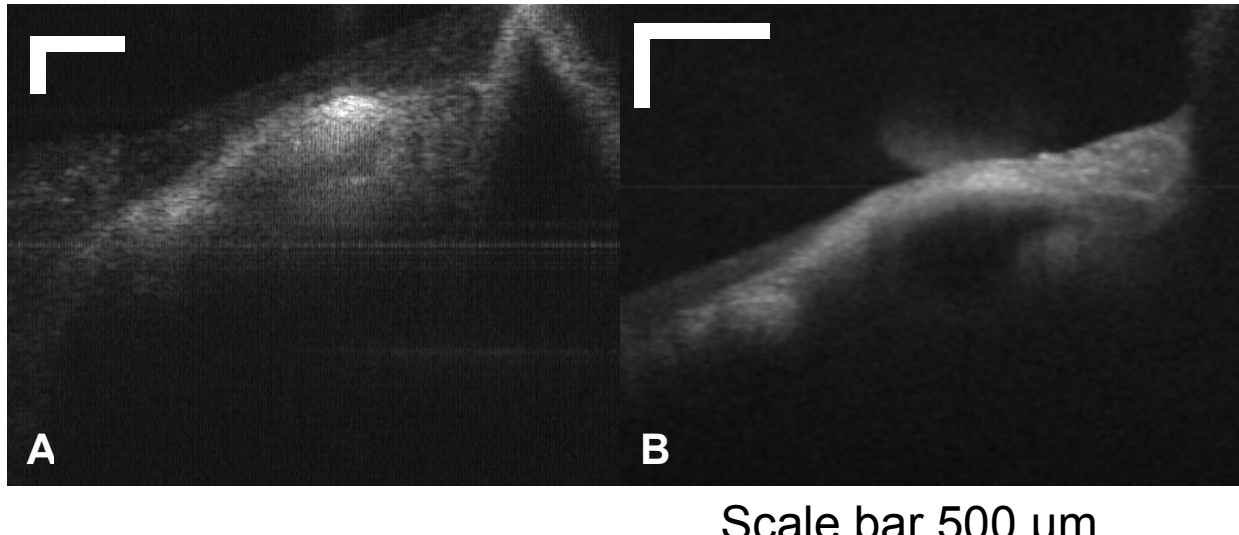
Email- btyler@jhmi.edu

Supplemental Figure I. Pre-study experimental trial of the handheld OCT image probe with example imaging of a human cadaver intracranial artery at the skull base. Technical details of the imaging probe have been previously published.¹ (a) Photograph of imaging probe revealing the stainless steel handpiece. (b) Human cadaver after pterional craniotomy revealing the clinical feasibility of imaging vasculature at the skull base. (c and d) Example cross-sectional OCT images of a human cadaver artery at the skull base acquired with the handheld probe (the solid material within the vessel lumen is the colored silicone latex injection, which was injected prior to assist with maintenance of vessel lumen patency during preservation and assist with vessel identification).



Scale bar 500 μm

Supplemental Figure II. Example pre-study experimental images of a live, *in vivo* mouse carotid artery with atherosclerotic plaque acquired both with an OCT benchtop system using a 1300nm light source and an 825nm light source. (a) Image acquired using a 1300nm light source. (b) Image of the same carotid artery at a similar location acquired using the 825nm light source reveals the greater detailed resolution of the proximal vessel wall.



Supplemental Video I: Cross-sectional OCT video of the carotid artery of the wild-type mice on regular diet. Mouse number 10 is imaged in these video clips. No carotid plaque is identified.

(a) Live, *in vivo* imaging of the mouse carotid. (b) *In situ* imaging of the mouse carotid after perfusion.

Supplemental Video II: Cross-sectional OCT video of the carotid artery of the Apolipoprotein E deficient ($\text{ApoE}^{-/-}$) mice on high fat diet. Mouse number 17 is imaged in these video clips.

Plaque is identified within the upper right portion of visualized artery. (a) Live, *in vivo* imaging of the mouse carotid. (b) *In situ* imaging of the mouse carotid after perfusion.

References

1. Zhang K, Huang Y, Kang JU. Full-range fourier domain optical coherence tomography imaging probe with a magnetic-driven resonant fiber cantilever. *Opt Eng.* 2011;50